Spin dynamics in beta -oxygen

1993 J. Phys.: Condens. Matter 5 6295

(http://iopscience.iop.org/0953-8984/5/34/016)

J. Phys.: Condens. Matter 5 (1993) 6295–6312. Printed in the UK

Spin dynamics in β-oxygen*

A Chahid†, F J Bermejo‡, A Criado§, J L Martínez¶ and M García-Hernández‡

† Departamento de Física de Materiales, Universidad del País Vasco, PO Box 1072, E-20080, San Sebastián, Spain

‡ Instituto de Estructura de la Materia, Consejo Superior de Investigaciones Científicas, Serrano 123, E-28006 Madrid, Spain

§ Departamento de Física de la Materia Condensada, Universidad de Sevilla, PO Box 1040, E-41080 Sevilla, Spain

¶ Instituto de Ciencia de Materiales, Sede B, Facultad de Ciencias, C-IV, Universidad Autónoma de Madrid, Cantoblanco, E-28049, Madrid, Spain

Received 20 April 1993, in final form 9 June 1993

Abstract. The magnetic and structure-related excitations in solid β-oxygen are investigated by means of high-resolution inelastic neutron scattering. An approximate separation of the magnetic response is achieved by means of modelling the structural excitations from a lattice dynamics calculation, and the reliability of such a separation assessed by comparison of the static magnetic susceptibility with that derived from polarized neutron diffraction. In addition, the analysis of the experimental strictly elastic intensity reveals the presence of static short-range magnetic order, evidencing the presence of two different characteristic correlation lengths.

1. Introduction

Solid molecular oxygen constitutes an interesting case example where the magnetic exchange interactions arise from direct overlap coupling of molecular orbitals belonging to different molecules [1]. Of the three known crystalline modifications [2], long-range antiferromagnetic order is certainly present in the low-temperature α-phase ($T < 23.9$ K at zero applied pressure), as evidenced by neutron diffraction [2], susceptibility measurements [3], muon spin rotation (μSR) [4] or antiferromagnetic resonance experiments [5]. On the contrary, the magnetic properties of the higher-temperature β-phase ($23.9 < T < 43.8$ K) remain somewhat controversial since the antiferromagnetic-like behaviour of the susceptibility [3] is not accompanied by the presence of (sharp) magnetic Bragg reflections [5,6], nor zero-field precession signals found in μSR experiments [4].

The crystal structure of the β-phase corresponds to a rhombohedral (hexagonal) $R\bar{3}m$ arrangement [2] (a schematic drawing is shown in the inset of figure 2), and several models have been brought forward to account for the magnetic structure† . Between such proposals,

* Work performed at the Institut Laue–Langevin.

† A triangular two-dimensional structure with nearest-neighbour interactions was proposed by Lotkev, and a quasi-helicoidal 2D model by Slyusarev and co-workers. A 3D model accounting for interplane interactions leading to a complicated magnetic phase diagram has been given by Jensen. The absence of MLRO can also be explained if a three-sublattice triangular antiferromagnet with some distortions (i.e. canting of spin directions in different domains) is considered; see Meier. A model of infinitely degenerate helices with the extremity of the propagation

0953-8984/93/346295+18$07.50

all those leading to magnetic long-range order (MLRO) such as the (unperturbed) triangular three-lattice antiferromagnet or those involving a strong coupling between different planes (3D order) seem to be at odds with polarized diffraction data [6], where a peculiar short-range helicoidal two-dimensional structure propagating perpendicularly to the crystal axis was proposed as the best model to explain the observed magnetic single-differential cross sections.

The purpose of the present work is to help to clarify the origin of the peculiar magnetic behaviour in β-oxygen, by giving some answers to the question of whether the magnetic correlations observed in this phase are of static or dynamic nature (or both), and, in the latter case, to validate the models brought forward to explain the static behaviour in terms of the corresponding dynamic correlations.

The dynamics of the higher-temperature plastic-crystal γ-phase ($43.8 < T < 54.4$ K) as well as the liquid up to temperatures near the boiling point were previously investigated [8] by means of the concurrent use of high-resolution inelastic neutron scattering (INS) and molecular dynamics (MD) simulations, something which enabled an approximate separation of the structure-related and magnetic responses. Although a polarized INS study of the β-phase has been previously reported [5], the fairly low resolution in energy transfers and the low counting statistics made the measurement of very limited use and only qualitative conclusions regarding the wavevector dependence of the measured intensity were derived from such a study. Our approach is somewhat similar to the one previously employed for the analysis of the orientationally disordered phases [8]. The structural excitations are accounted for by means of a molecular Born–von Karman lattice dynamics (LD) calculation [9], and in order to check the adequacy of the separation of magnetic and structural responses, the static wavevector-dependent magnetic susceptibility is calculated and compared with that measured by polarized neutron diffraction [6]. As in the previous work, the coupling between structural and magnetic excitations is assumed to be weak (as a matter of fact only in the low-temperature range of existence of the α-phase was the presence of noticeable magneto-vibrational coupling inferred [5]), and therefore the magnetic properties as calculated from the isolated magnetic spectral response should serve as an indication of the adequacy of the decoupling approximation.

Some relevant details concerning the measurement and calculational procedures are given in section 2, and the main results described in section 3. A general discussion regarding the relevance of the present findings as well as the main conclusions are drawn in section 4.

2. Experimental and computational details

2.1. Experiments

The experimental conditions and data correction procedures have been described in our previous work on the plastic-crystal and liquid phases [8], and therefore only a brief description is given here. The measurements were carried out using the IN6 spectrometer located at the Institut Laue–Langevin (ILL, Grenoble, France), and the results presented in this work correspond to a temperature of $T = 35$ K, the same at which the polarized diffraction experiment of [6] was performed (measurements at thermodynamic conditions

vectors also describing an helix in reciprocal space has been developed by Rastelli and co-workers. The analysis of the polarized neutron diffraction data of [6] favours a 2D helical structure with an angle between neighbouring moments of 141°. All these references are given in [7].

corresponding to higher-temperature phases have already been reported [8]). The incoming neutron energy was of 4.189 meV (incident wavelength $\lambda = 4.12\,\text{Å}^{-1}$), and the resolution in energy transfers as measured with a vanadium standard was of 0.06 meV (HWHM).

The absorption corrections were applied using a modification of the SLABS code to account for cylindrical geometries [10], and the multiple-scattering contributions were evaluated from Monte Carlo calculations performed with the DISCUS code [11]. The maximum percentage of multiply scattered neutrons never exceeded six per cent. The corrected spectra were then converted into constant Q by means of the INGRID code [12].

Unlike the case of the plastic-crystal γ-phase, single-crystal samples of the low-temperature phases of oxygen are extremely difficult to prepare due to the large contraction in molar volume which occurs at the γ–β transition ($\approx$ 5%). However, previous measurements [1,5] have evidenced the essentially isotropic character of the magnetic susceptibility in the β-phase, something which in turn alleviates the need of single-crystalline specimens.

A representative set of spectra corresponding to wavevectors below the maximum of the peak of the magnetic single differential cross section ($\approx 1.3\,\text{Å}^{-1}$) [6], near the maximum, and above it is shown in figure 1.

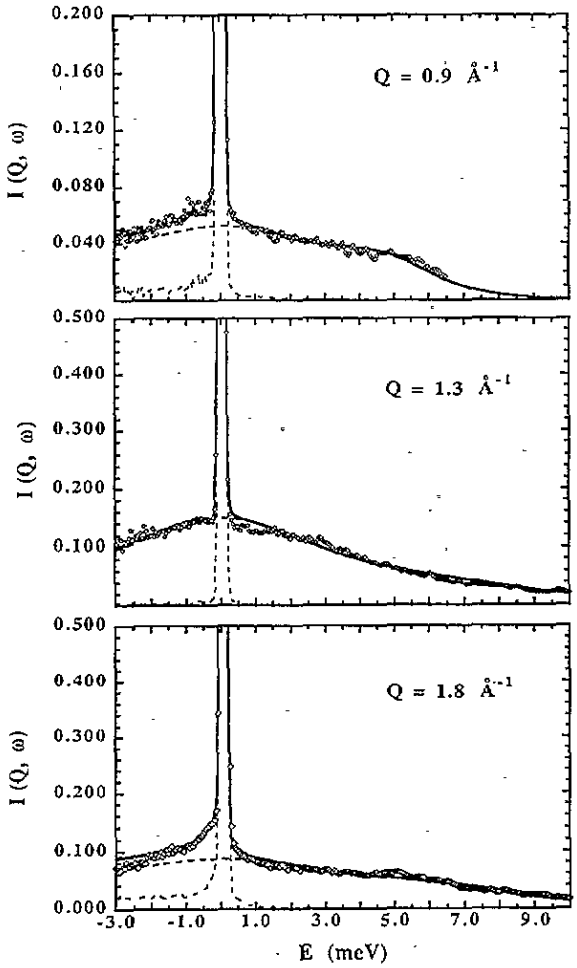

Figure 1. A comparison of experimental (diamonds) and fitted (full curve) constant-Q spectra for momentum transfers below (0.9 Å^{-1}), about the maximum of the magnetic static structure factor (1.3 Å^{-1}), and above (1.8 Å^{-1}). The resolution function as measured from a low-temperature (4 K) sample is shown by the broken curve. The broad component shown by the broken curve represents the $I_m(Q,\omega)$ magnetic intensity.

2.2. Lattice dynamics

The structure-related excitations can be modelled by either molecular or lattice dynamics calculations. The advantage of the former approach lies in the account of possible anharmonic contributions, which become increasingly important for relatively high temperatures. In contrast, the statistical accuracy of the calculated functions, particularly for space-dependent properties, are far poorer when this approach is used due to finite-size effects. For such a reason, and in order to deal with relatively low intensities, we have chosen to follow the second approach, which is better suited for problems with translational invariance. A lattice dynamical calculation has been carried out at the energy-minimized crystal configuration using our own computer code [9], and the relevant details concerning the employed potential as well as its validation are given in our previous contribution [8]. Details concerning this kind of calculation for molecular materials have already been given, and the interested reader should consult, for example, [13].

From the solution of an eigenvalue equation, the vibrational frequencies $\omega(\boldsymbol{q})$ and polarization vectors $e(\boldsymbol{q})$ for wavevector $\boldsymbol{q}$ are computed, and the coherent inelastic neutron scattering intensity $S(\boldsymbol{Q}, \omega)$ is calculated afterwards within the one-phonon approximation for dispersion vectors $\boldsymbol{Q}$, obeying $\boldsymbol{Q} = \boldsymbol{G} - \boldsymbol{q}$ and $E - E_0 = \pm\hbar\omega(\boldsymbol{q})$, where E and E_0 are the energies of the dispersed and incident neutrons respectively, $\boldsymbol{G}$ is a reciprocal lattice vector and $\omega(\boldsymbol{q})$ is the frequency of the phonon $(\boldsymbol{q}_j)$ involved in the process.

For the polycrystal, the relevant scattering function $S_{\text{nuc}}(Q, \omega)$ must be obtained as an average of $S(\boldsymbol{Q}, \omega)$ over all scattering directions $\boldsymbol{Q}$ [14]. This process has been carried out by dividing the Q space into a fine mesh ($40 \times 40 \times 40$ points in the first Brillouin zone).

The $Z(E)$ crystal frequency distribution function (DOS) has been calculated by means of a sampling over the crystal Brillouin zone using a mesh of $18 \times 18 \times 18$ points along each reciprocal lattice direction.

The experimental intensity was therefore analysed in terms of a sum of structure-related and magnetic dynamic structure factors as

$$I(Q, \omega) = A(Q)[S_{\text{nuc}}(Q, \omega) + I_{\text{m}}(Q, \omega)] \otimes R(Q, \omega) \tag{1}$$

where $A(Q)$ is a scaling constant (required since the measured quantities could not be obtained in absolute units), $S_{\text{nuc}}(Q, \omega)$ is the dynamical structure factor evaluated from the LD results as explained above, $R(Q, \omega)$ is the instrumental resolution function (measured from low-temperature (4 K) runs) and the magnetic response is given by

$$I_{\text{m}}(Q, \omega) = (\gamma e^2/m_e c^2)^2 |\tfrac{1}{2} g f(Q)|^2 S_{\text{m}}(Q, \omega) \tag{2}$$

being $(\gamma e^2/m_e c^2)^2 = 0.291$ barns, the neutron–magnetic system coupling constant, $g = 2$ is the Landé factor (quenched orbital momentum) and $f(Q)$ is the molecular form-factor which was taken from [6].

Since the inelastic intensity arising from phonon excitations is accounted by the $S_{\text{nuc}}(Q, \omega)$ term, a model for the lineshapes of $S_{\text{m}}(Q, \omega)$ is required to perform parametric fits to the experimental intensities, and some details are given in the next section. In order to investigate the dependence of the magnetic response with the specific functional form chosen to isolate it, two models were tested as far as the form on $S_{\text{m}}(Q, \omega)$ dynamic spin correlations is concerned, and the relevant results are described below.

3. Results

As a first step in the analysis, it is instructive to compare the magnetic response of the β- and plastic-crystal γ-phases, as derived from polarized neutron diffraction [15], and shown

in figure 2. The most remarkable differences between the magnetic diffraction profile of the β- and γ-phases concern the shift of the maximum towards a somewhat larger Q-value in the β-phase ($\approx 1.3\,\text{Å}^{-1}$ against $\approx 1.1\,\text{Å}^{-1}$), a smaller width, indicating a larger coherence length, and a faster decay towards the hydrodynamic limit, in accordance with the smaller value of the magnetic susceptibility [3].

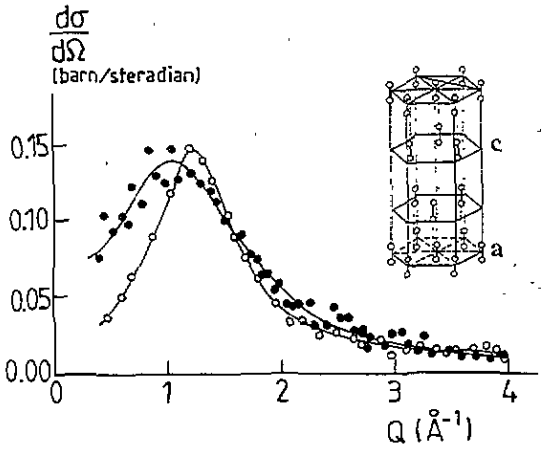

Figure 2. The energy-integrated magnetic single-differential scattering cross section for γ-(filled circles) and β- (open symbols) oxygen, as measured by polarized neutron diffraction [6, 15]. The full curves are drawn as guides to the eye. The crystal structure of β-oxygen is shown schematically in the upper part of the figure.

3.1. Structural and magnetic form factors

The existence of a clear magnetic response at finite wavevectors can be gauged from figure 3, where the experimental intensities $I(Q, \omega = ct)$ are shown for several values of the momentum transfer alongside the $S_{\text{nuc}}(Q, \omega = ct)$ functions as calculated from the LD results. As can be seen from the graph, a well defined peak centred at $\approx 1.3\,\text{Å}^{-1}$ in the experimental data starts to develop at energy transfers as low as 0.25 meV. For 1 meV and up until 5 meV such a feature remains very clearly visible, and becomes increasingly difficult to separate from the phonon background for energy transfers of 6 meV and above. In counterposition, a comparison between the structure-related and magnetic structure factors, as shown in the graphs, reveals the phononic origin of some of the prominent peaks appearing in the experimental functions, such as the intense response at about $Q \approx 2.2\,\text{Å}^{-1}$ for energy transfers below 5 meV, or some smaller features appearing as bumps in the experimental spectra such as the peak at $1.7\,\text{Å}^{-1}$ for the curve corresponding to 0.5 meV of energy transfer. It is therefore rather gratifying that the main peaks appearing in the calculated functions can be scaled to reproduce the parts of the experimental curves that are of a structure-related origin. Such a fact ensures that the analysis of the observed intensities based upon the decoupling of magnetic and structural degrees of freedom can be carried out at least on semiquantitative grounds.

In order to contrast the predictions made by Rastelli and co-workers [16], regarding the appearance of a sawtooth-like diffraction (strictly elastic) profile, figure 4(*a*) shows the wavevector dependence of the strictly elastic intensity for all three solid phases of oxygen. The referred authors have developed a model for a rhombohedral Heisenberg antiferromagnet (RAF) [16], for which β-oxygen appears as a convenient physical realization. The higher resolution in energy transfers achieved in the present experiment (≈ 0.06 meV, about one order of magnitude higher than that of previous studies [5]), enables the isolation of this

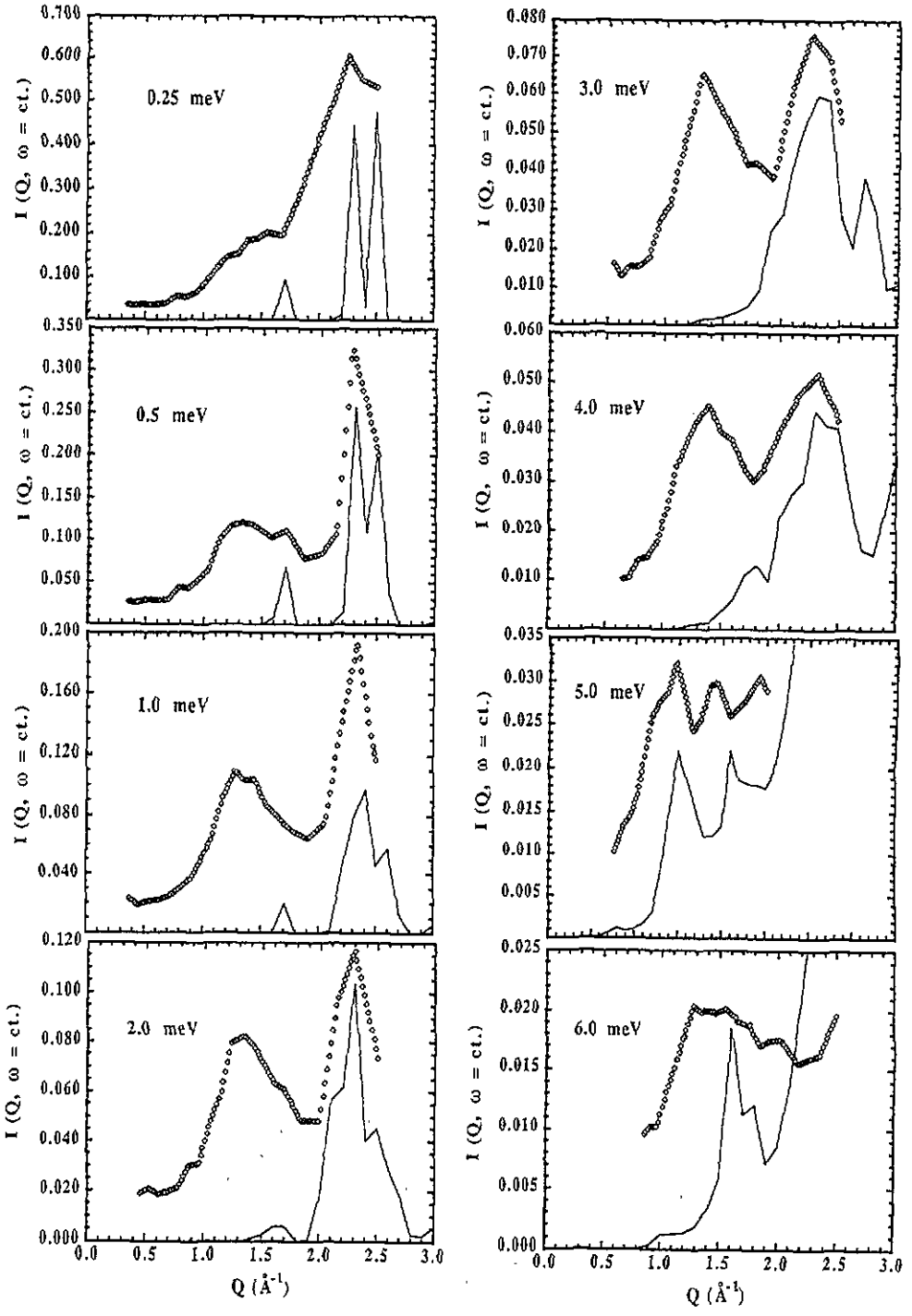

Figure 3. A comparison between the experimental (open diamonds) inelastic intensities for several values of the energy transfer (given in the upper left part of the graph) with the nuclear (structure-related) intensities as calculated from the LD results. The LD spectra have been scaled to the experimental results using a common value for the $A(Q)$ scaling constant of (1).

spectral component and thus provides a direct test of the theoretical predictions. As can be seen from the figure, the magnetically ordered α-phase shows a strong line of magnetic origin corresponding to the $(\bar{1}01)$ Bragg reflection, centred at about 1.35 $Å^{-1}$ with a small feature alongside at about 0.84 $Å^{-1}$ which has not been indexed in any of the previous diffraction studies, and cannot correspond to a Bragg reflection of nuclear origin. In counterposition, the β-phase shows two broad features centred at about $Q \approx 0.84$ $Å^{-1}$ and $Q \approx 1.10$ $Å^{-1}$, followed by the strong (003) nuclear Bragg reflection. The proof that the small feature at 0.84 $Å^{-1}$ does not arise from sample-independent effects is given by its absence in the γ plastic-crystal phase, where only a broad background of diffuse-scattering origin is seen. A comparison with the profile calculated from the RAF model is also given in figure 4(*b*) where, as can be judged from the comparison, both the peak position and shape of the experimental function are clearly at odds with the calculation.

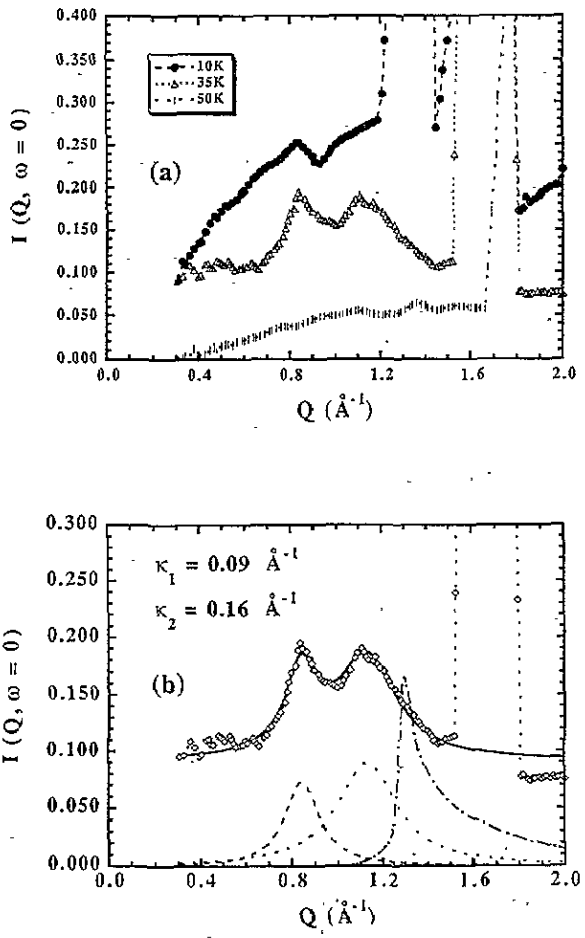

Figure 4. (*a*) The upper part shows the $I(Q, \omega = 0)$ strictly elastic intensities representing integrated quantities for energy transfers within 0.08 meV for the α-phase at 10 K (filled circles), the β-phase at 35 K (open triangles) and the γ plastic crystal at 50 K (bars). The presence of the strong $(\bar{1}01)$ magnetic Bragg reflection at about $Q \approx 1.35$ is seen in the α-phase followed by the stronger (001) curve of nuclear origin. The intensity of the magnetic $(\bar{1}01)$ Bragg reflection is about 12 times stronger than the small feature located at about $Q \approx 0.84$ $Å^{-1}$. Strong Bragg curves of nuclear origin are also seen at $Q \approx 1.7$ $Å^{-1}$ and $Q \approx 2.1$ $Å^{-1}$ in the other phases. (*b*) The lower frame shows a fit of the low-Q part of the $I(Q, \omega) = 0$ static function using (3), (4) and the resulting values for the inverse correlation length are shown in the upper left side. The two individual Lorentzian components are shown at the bottom alongside with the shape for the structure factor as calculated from the RAF model [16] (chain curve).

What seems very relevant regarding figure 4(*a*) is the fact that the broad feature located at $Q \approx 0.84$ $Å^{-1}$ in both the α- and β-phases corresponds to a distance in real space of about 7.5 Å, which is roughly twice the interplanar spacing in the α-phase and also the distance

from a molecule on the basal plane and another located in the plane containing next-nearest-neighbour molecules in the rhombohedral β-phase (i.e. the distance from planes a and c in the drawing shown in figure 2).

An analysis of the two features appearing in the $I(Q, \omega = 0)$ function corresponding to the β-phase in terms of the Ornstein–Zernike approximation [17] is also shown in figure 4(*b*). As can be seen from the figure, the elastic pattern up the base of the (003) reflection can be well reproduced by two Lorentzians plus a flat background such as

$$I(Q, \omega = 0) = b + \sum_{i=1,2} I_i(Q, \omega = 0) \tag{3}$$

$$I_i(Q, \omega = 0) = a_i \frac{\kappa_i}{(Q - q_i)^2 + \kappa_i^2} \tag{4}$$

where a_i is an amplitude factor related to the second moment of the exchange function (i.e. $a_i \approx \sum_n n^2 J(n)$), κ_i denotes the inverse correlation length of the ith Lorentzian (HWHM) and q_i denotes the position of the peak maxima. The values found for κ_1 and κ_2 as given in the figure indicate that the correlation length of the Lorentzian centred at $Q \approx 0.84\,\text{Å}^{-1}$ is $\xi_1 \approx 11.2\,\text{Å}$, whereas the one centred at about $Q \approx 1.13\,\text{Å}^{-1}$ corresponds to a length of about $\xi_2 = 6.25\,\text{Å}$†.

There have been some marked disagreements regarding the correct value of the correlation length in β-oxygen. From total diffraction as well as from model-building considerations [2, 7], some authors have given values of about 12 Å for this quantity, whereas a lower estimate of about 5 Å was proposed from the analysis of polarized diffraction data [6]. On the contrary, Stephens and co-workers [5] gave a value in between those quoted above, 9 Å from the analysis of the quasielastic intensities in a low-resolution experiment. In contrast, the present results seem to indicate that static magnetic short-range order is present, and the peak at lower wavevectors ($Q \approx 0.84\,\text{Å}^{-1}$) can be interpreted, from consideration of the distances involved ($\approx 7.5\,\text{Å}^{-1}$) and the crystal structures of the two lower-temperature phases, as arising from weak interplanar coupling in both the long-range ordered α-phase as well as in the β-phase.

The peak at $1.13\,\text{Å}^{-1}$ appearing in the β-phase probably arises from correlations between next-nearest neighbours within the hexagonal planes. In fact the distance which corresponds to this value, $5.69\,\text{Å}^{-1}$, coincides with that separating parallel spins in a triangular three-sublattice Heisenberg antiferromagnet [7]. Additional support for such an assignment comes from the comparison of the α- and β-patterns, where the absence of this peak in the former phase is explained by the presence of a strong magnetic Bragg reflection. To summarize, what the analysis of the $I(Q, \omega = 0)$ intensities has revealed is the presence of static magnetic order in the β-phase. Previous diffraction studies have been unable to reveal this feature due to the strong paramagnetic background which, once integrated in energy, will produce a peak shape as depicted in figure 2, a reminiscence of which is clearly seen in some of the curves shown in figure 3.

3.2. Spectral lineshapes

The spin dynamics of the γ-phase as well as the liquid were considered in a previous work [8], where the magnetic correlations were analysed in terms of a model for an

† Because of the difficulty in estimating the resolution in wavevectors in a time-of-flight instrument, the values given for the correlation lengths should be considered as lower bounds. However, on qualitative grounds an estimate of this quantity can be obtained from analysis of the width of the peak corresponding to the lowest magnetic Bragg reflection, which gives a value of $0.03\,\text{Å}^{-1}$. An upper bound for this quantity can be estimated by assuming a Lorentzian resolution function with this linewidth, giving $\xi 1, 2 \approx 16\,\text{Å}$ and $\approx 8.3\,\text{Å}$ respectively.

exchange-coupled paramagnet, something which was able to reproduce satisfactorily the spectral lineshapes after accounting for the structure-related excitations as mentioned above. From the test of different models against the polarized neutron cross section it has been argued [6, 15] that only two-dimensional models with correlations extending up to second neighbours are fully compatible with the experiment. Additionally, a purely paramagnetic contribution with a substantial amplitude ($\approx$ 15%) was added to improve the fits (in opposition, the analysis of the macroscopic susceptibility revealed the scarce importance of molecular diamagnetic and Van Vleck contributions [1, 3]). The approach followed for the analysis of the magnetic diffraction intensities [6] accounted the absence of Bragg reflections of magnetic origin by means of introducing a Lorentzian spread function [5, 6] characterized by an adjustable parameter $\kappa = 1/\xi$ taken to be equal to the inverse correlation length. The approach followed in the present work is somewhat more general since models for the $S_m(Q, \omega)$ are directly tested against the total experimental intensities and, as will be seen below, the zeroth-frequency moment of such a quantity (i.e. the static magnetic structure factor), are in reasonable agreement with the experimental functions as measured in the polarized diffraction experiments.

Two models have been tested for the analysis of the experimental data. The first one corresponds to an exchange-coupled (Heisenberg) paramagnet and is used along the same lines as those described for the analysis of the γ- and liquid phases [8]. Such a model which approximates the magnetic spectral weight function $F(Q, \omega)$ by means of a three-pole formula, has been thoroughly employed for the analysis of critical magnetic fluctuations in metallic or insulating paramagnets [18] is completely defined once the quantities ω_0 and ω_s, related to the second- and fourth-frequency moments ($\langle\omega^2\rangle = \omega_0^2$, $\langle\omega^4\rangle = \omega_0^2\omega_s^2$), as well as to the static susceptibility χ_Q, as

$$S_m(Q, \omega) = \omega/[1 - \exp(-\hbar\omega/k_B T)]\chi_Q F(Q, \omega) \tag{5}$$

$$F(Q, \omega) = \tau\omega_0^2(\omega_s^2 - \omega_0^2)/\pi[\tau\omega(\omega^2 - \omega_0^2)^2] \tag{6}$$

with a relaxation time $\tau = [\pi(\omega_s^2 - \omega_0^2)]^{1/2}$.

The second model considered here treats the magnetic response in purely hydrodynamic terms, following the same approach as that used to analyse the spin dynamics of two-dimensional antiferromagnets in their paramagnetic phases [19]†

$$S_m(Q, \omega) = \chi_m\omega/[1 - \exp(-\hbar\omega/k_B T)]\left(\frac{\Gamma_m}{\Gamma_m^2 + (\omega - \omega_m)^2} + \frac{\Gamma_m}{\Gamma_m^2 + (\omega + \omega_m)^2}\right) \tag{7}$$

where the frequency dependence of the magnetic response is characterized in terms of an average frequency ω_m and damping constant Γ_m.

The procedure to isolate the magnetic response was therefore to fit the experimental data taken as constant-Q spectra with the model $I(Q, \omega)$ specified by (1), using the four-parameter vectors $\Theta = (A(Q), \chi_Q, \omega_0^2, \omega_s^2)$, when the first model for the spin dynamics was

† The double-Lorentzian function used in [19] and also in this paper seems to lack an adequate theoretical justification since a rigorous derivation from anharmonic phonon theory will lead to a function for a harmonic oscillator which can be cast as a difference of two equal-breadth Lorentzians. See for instance Domer, and also Fåk, [20]. The results when this approach is used, considering a difference of two Lorentzians, are only slightly different specially at Q values below $Q \leqslant 0.8\,\text{Å}^{-1}$, where some quasielastic intensity has to be added to reproduce the experimental data. Such small differences can be understood if consideration is made of the fact that only overdamped excitations (i.e. the Γ_m damping constants) largely exceed the ω_m frequencies. The rationale behind the use of the function given by (7) was to provide a comparison with experimental and computer simulation analysis on systems described above [19], which have been carried out using such formula.

considered, and $\Theta = (A(Q), \chi_m, \Gamma_m, \omega_m)$ for the double-Lorentzian model. Note that since the basic test employed to assess the reliability of the isolation procedure was to compare the (energy-integrated) static susceptibility with that measured by polarized diffraction, the quantities χ_Q and χ_m were left as adjustable parameters.

Some examples regarding the quality of the fits to the experimental data using the first approach were shown in figure 1. Although the fits to the experimental intensities were somewhat poorer when using the second (hydrodynamic) approach, the characteristic linewidths Γ_m turned out to be roughly the same as those estimated from the three-pole formula, calculated from the ratio of second- and fourth-frequency moments as $\Gamma_Q = \pi/2[\langle\omega^2\rangle^3/\langle\omega^4\rangle^4]^{1/2}$, as is shown in figure 5, and the same qualifications also apply the frequency integral over $S_m(Q, \omega)$. What seems then clear from the comparison of results derived from both models is that the $S_m(Q, \omega)$ conforms to a description in terms of paramagnetic fluctuations, leading the two models to broad frequency distributions with equal width. The possible presence of finite-frequency features cannot be ruled out from the three-pole formula, although it seems clear from the second approach that, if they exist, they should be subjected to very strong damping (or overdamping) conditions.

Another interesting thing to note is the fact that, as also shown in figure 5, the frequency integral over the magnetic response (i.e. $\int_{E_c}^{E_c} d\omega\, I_m(Q, \omega)$, with $E_c = 10$ meV) gives rise to a broad peak centred at about $Q \approx 1.3\text{Å}^{-1}$ with a shape in tolerable agreement with that isolated by means of polarized total scattering [6]. The main disagreements between the function derived from polarized total scattering (diffraction) and the present result concern the low- and high-Q sides of the curve, where the isolation of the magnetic spectra become less reliable. In the first case, the lower intensity of the low-Q part of the present result does not extrapolate to the correct value of the static quantity, which according to [15] should be of 0.0318 barns per sterad. Such a deficiency arises from the very limited dynamic range below $Q \approx 0.7\,\text{Å}^{-1}$ accessible through cold neutron spectroscopy under the conditions employed in the present experiment, something which makes difficult the isolation of the magnetic response for these relatively low-momentum transfers. On the other hand, for momentum transfers $Q \geqslant 1.6\,\text{Å}^{-1}$, the magnetic response is characterized by a rather broad Lorentzian of increasing width (see figures 5(*b*) and 5(*d*) covering a range of energy transfers, which becomes comparable (or larger than) the one allowed by the kinematics of the present experiment. Apart from lending further support to the present approach to isolate the magnetic response, such a fact reveals that the energy-integrated diffraction measurements reported up to date [2] have masked the presence of the two small peaks visible in the $I(Q, \omega = 0)$ function.

The above-referred curves (frequency integrals of the magnetic response) can be interpreted in terms of initial-time ($t = 0$) wavevector-dependent susceptibilities which once cast, as before, into an Ornstein–Zernike form can be expressed in terms of a κ_0 inverse correlation length. The calculated value for this quantity now gives $0.24\,\text{Å}^{-1}$ for the inverse correlation length, which corresponds to a distance of 4.2 Å, also in tolerable agreement with the value of 5 Å derived by Dunstetter from the analysis of the polarized diffraction experiment. What it is worth remarking at this point is the fact that the value of such a characteristic length estimated from the frequency integrals of the magnetic response is substantially smaller than that for $\xi_{1,2}$ estimated from the static (i.e. $t = \infty$) response of 11.2 Å and 6.25 Å given above.

A sample of the structure-related and magnetic responses isolated in such a way is shown in figure 6. As expected the nuclear $S_{nuc}(Q, \omega)$ functions show a rich structure with a strong Q-dependence, a sample of which is also given in the inset of the figure, where the

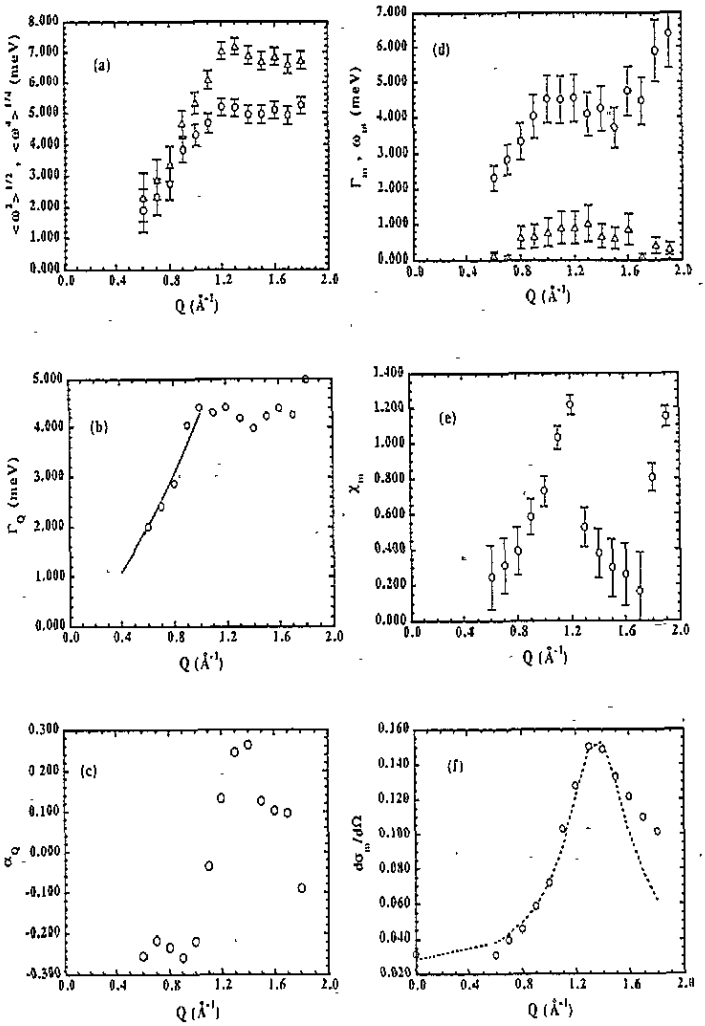

Figure 5. Lineshape parameters defining the $S_m(Q,\omega)$ magnetic dynamic structure factors. The left column portrays the results of the analysis in terms of the exchange-coupled Heisenberg paramagnet (5), (6). (*a*) The reduced second $\langle\omega^2\rangle^{1/2}$ (circles) and fourth $\langle\omega^4\rangle^{1/4}$ (triangles) frequency moments of the scattering law. (*b*) The Γ_Q linewidths of an equivalent Lorentzian, as calculated from the ratio of second to fourth moments (see text) are given as circles, and the full curve shows the approximation in terms of the $D_s Q^{3/2}$ law as described in section 4. (*c*) The α_Q lineshape parameter as calculated from the frequency moments. (*d*) and (*e*) show the wavevector dependence of the parameters arising from fits to the model given by (7). (*d*) shows the wavevector dependence of the ω_m frequencies (open squares) and Γ_m damping factors (open circles). (*e*) displays the amplitude factors χ_m of (7). (*f*) shows the (energy-integrated) single-differential cross section calculated from integrals of the model functions corresponding to the exchange-coupled paramagnet (open circles). Units are barns/sterad and the experimental data have been scaled to that measured by polarized diffraction as shown in figure 2. The data point at $Q = 0$ corresponds to the macroscopic value for the susceptibility as taken from [15]. The broken curve corresponds to the best approximation to the data using an Ornstein–Zernike form.

frequencies of the more intense peaks are plotted against the wavevectors, and the correct

approach to the hydrodynamic limit is shown. In counterposition, the magnetic response is encompassed by broad frequency distributions showing an apparent shoulder at low wavevectors. Because of the kinematical restrictions of the present experiment, it becomes rather difficult to assess the physical soundness of such a marked shoulder. The general shape of the curves, even for large wavevectors, is reminiscent of those found for well known paramagnets such as EuO or EuS [18] (i.e. the spectra are too 'square' compared with that of purely overdamped excitations). An estimate of the Q-region where finite-frequency features can be present is given, for the paramagnetic model, by the parameter $\alpha_Q = \frac{1}{3}[(\omega_s^2 - \omega_0^2)/\omega_0^2 - 2]$, which takes negative values [8] corresponding to real roots for the model eigenfrequencies. As shown in figure 5, a small range of Q covering up to $\approx 1\,\text{Å}^{-1}$ fulfils this criterion, although as mentioned above it rather unfortunately coincides with the Q-range where the isolation of the magnetic response is less reliable.

3.3. Frequency distributions

As a means to compare the spectral distribution of structure-related and magnetic excitations, figure 7 displays the $Z(E)$ vibrational density of states as calculated from the LD results described above, alongside with that computed from the $S_m(Q, \omega)$ magnetic response functions. For such a purpose the density of states for magnetic excitations is considered following the general arguments which for disordered magnetic systems are given in [21]. Since to the authors' knowledge no well established procedure seems to have been reported concerning the derivation of this quantity from the $S_m(Q, \omega)$ functions, we have followed a procedure along the same lines as that initially proposed by Buchenau [22] for the calculation of this quantity for a disordered system from the measured inelastic intensities arising from structure-related excitations within the incoherent approximation

$$Z_m(E) \propto \frac{\omega S_m(Q, \omega)}{n(\omega)\hbar Q^2 \exp(-2W)}$$

where $n(\omega)$ is the Bose factor, and the value of the Debye–Waller factor is set to the same value as that derived from total diffraction measurements ($0.012\,\text{Å}^{-2}$) [2].

The comparison of $Z(E)$ and $Z_m(E)$ displayed in figure 7 shows that for the temperature range of interest (up to about 5 meV) the magnetic $Z_m(E)$ function shows small deviations from linearity in E, and only a broad maximum is apparent at about 8 meV. The presence of such extrema mainly arises from the strong damping effects and cannot be considered as a clear signature of the existence of well defined spin excitations. The spectrum shown in the figure has some resemblance with that calculated by Kirkpatrick and Harris for a disordered quasi-two-dimensional antiferromagnet [23], and its relevance to explaining some of the relevant thermodynamic quantities is analysed in the next section. On the other hand, the $Z(E)$ calculated from the LD results shows a nearly quadratic dependence with frequency up to about 4 meV and a strong peak of mostly rotational character centred at about 5 meV.

4. Discussion and conclusions

4.1. Magnetic structure

The present work has given evidence that both static short-range order magnetic correlations as well as other of dynamic nature are indeed present in the orientationally ordered β-phase of condensed oxygen. The existence of a static magnetic order was not evidenced in previous

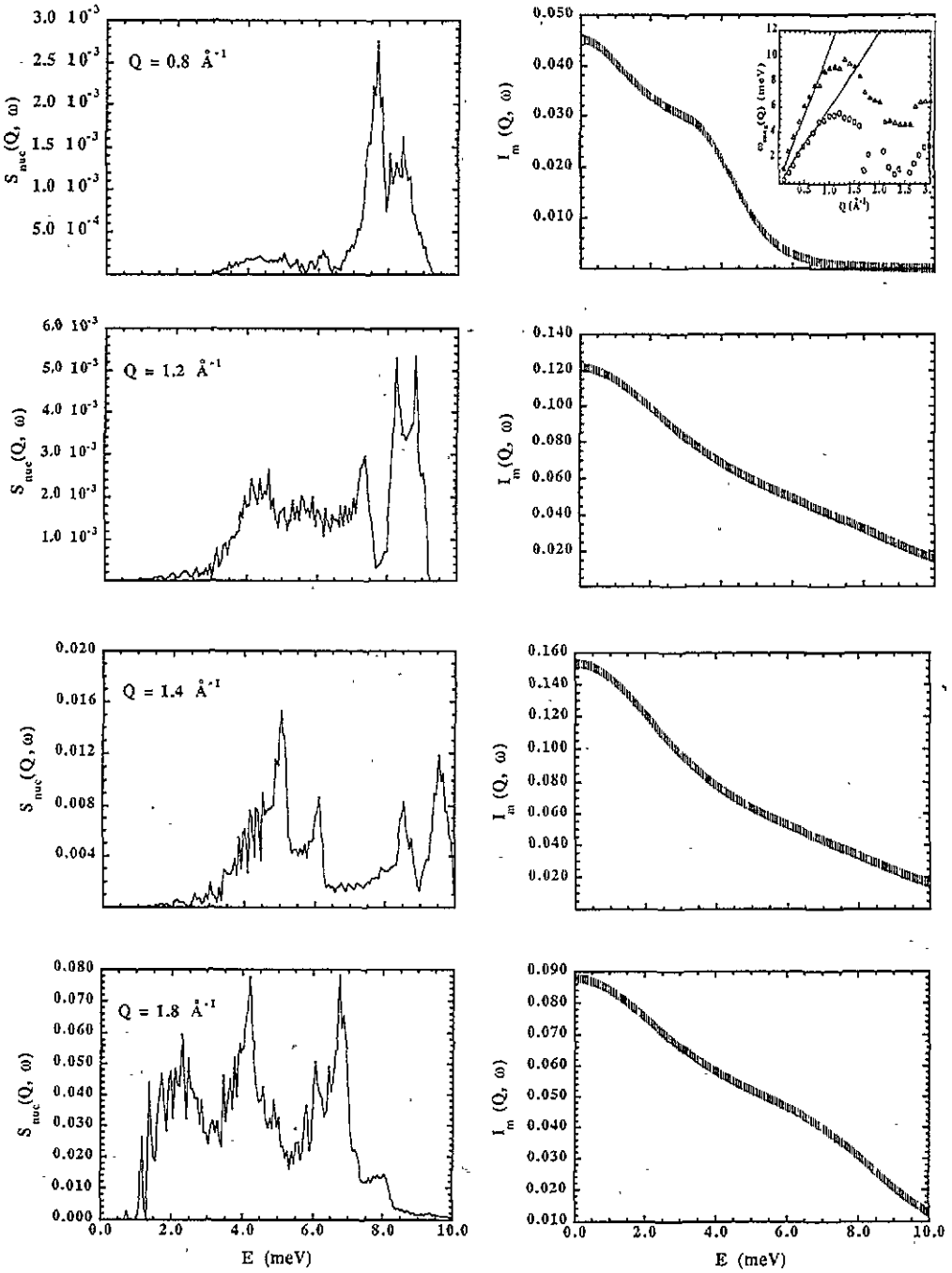

Figure 6. LHS: $S_{\mathrm{nuc}}(Q,\omega)$ dynamic structure factors as calculated after the polycrystalline average of the LD results for several values of momentum transfer (upper LHS). Bose factors are not included in order to show high-frequency components. RHS: corresponding $I_{\mathrm{m}}(Q,\omega)$ magnetic intensities. Inset in the upper RHS: wavevector dependence of the ω_{max} frequencies appearing in plots of $\omega^2 S_{\mathrm{nuc}}(Q,\omega)$. The two straight lines correspond to the dispersion of hydrodynamic sound.

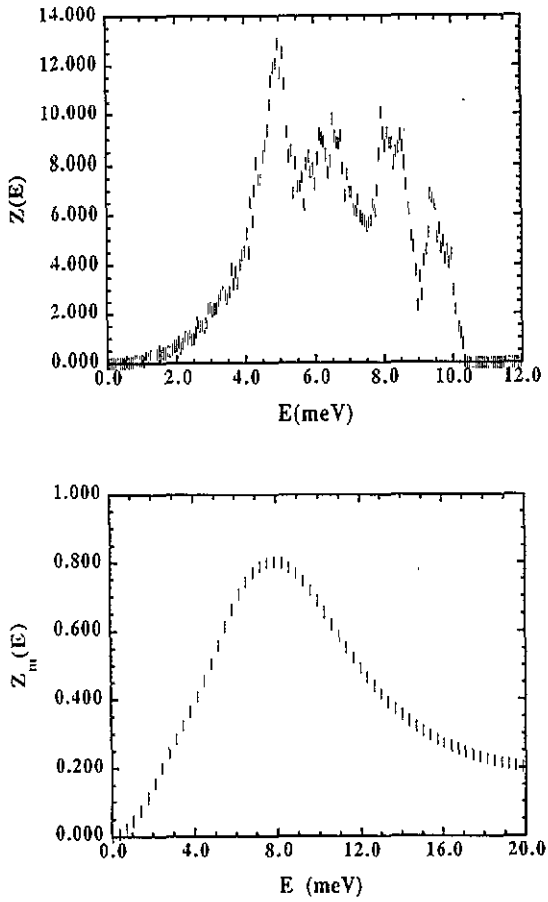

Figure 7. The upper frame shows the $Z(E)$ generalized frequency distribution (vibrational density of states DOS) as calculated directly from the LD results. The curve is normalized to $6R$. The lower frame shows the estimate of the $Z_m(E)$ frequency distribution for the magnetic excitations as calculated using (8). The curve is normalized to the corresponding value of $3R/2$.

experimental investigations since the presence of strong paramagnetic fluctuations masked the two small peaks appearing in the $I(Q, \omega = 0)$ pattern.

The nature of the magnetic order in β-oxygen has been a matter of a considerable debate for a number of years. The case brought forward by Rastelli and co-workers [16] seemed to encompass a realistic possibility since the absence of characteristic Bragg reflections evidencing the presence of 3D magnetic LRO was attributed to the infinite degeneracy of the ground state (the model predicts the presence of infinite degenerate 3D helices). The present results constitute the only experimental benchmark for such a prediction, due to its static nature, and as has been shown above, a strong disagreement between calculation and experiment is noticed (see figure 4(*b*)).

The assignment of the two peaks in the static function as arising from short-range interplanar and intraplanar correlations can contribute to provide an answer to the long-standing question of how a macroscopically antiferromagnetic solid does not exhibit strong magnetic Bragg reflections. From the estimated correlation lengths, it seems that the intraplanar correlations ($\xi_2 = 6.25$ Å) are more strongly affected by both paramagnetic fluctuations and some static kind of disorder than those of interplanar origin ($\xi_1 = 11.2$ Å). Such an assignment thus portrays β-oxygen as a system of quasi-two-dimensional magnetism, where the stronger interactions are expected to take place within the planes because of the strong dependence of the exchange constant with the intermolecular

separation (values of the intraplanar exchange constant of about 25 K (2.16 meV) are needed to explain the macroscopic susceptibility data, and are also reported in quantum-chemical calculations on oxygen dimers [24]), but these occur on a strong thermally excited background leading to a substantial amount of spin diffusion.

On the other hand, the present results give additional support to the existence of a triangular three-sublattice antiferromagnetic arrangement, and the question of the absence of long-range order of the magnetic moments seem now to be related to some random distribution of canting angles between different correlation domains. If this were not the case, as proposed by Dunstetter [6], some fingerprints of the modulated structure given in [6] should be readily apparent in the derived $Z_m(E)$ function [25], something which seems to be at odds with the results reported herein.

4.2. Paramagnetic fluctuations

If the measured broad inelastic background is interpreted in terms of a spin-diffusion mechanism characteristic of an exchange-coupled paramagnet, an estimate of the D_s spin-diffusion constant can be obtained from the low-Q portion (below 1 Å^{-1}) of the Γ_Q (or Γ_m) linewidth against momentum-transfer curves. As in the case of the higher-temperature γ-phase solid [8], such magnitudes seem to follow a $D_sQ^{3/2}$ behaviour characteristic of antiferromagnets at the critical point, more closely than a simple diffusion D_sQ^2 law. The values for the D_s diffusion constants estimated in such a way are 4.8(4) meV Å$^{3/2}$ for the former case and 5.3(9) meV Å^2 for the diffusion case which shows a far poorer fit (the χ^2 statistic is about one order of magnitude worse). Although at low momentum transfers $Q \leqslant 0.6$ Å^{-1}, the accurate determination of the magnetic linewidths becomes difficult due to the limited range of energy transfers, the fact that both sets of analysis lead to the same functional dependence with Q gives further support to the deviation from simple diffusive behaviour. The present values for the spin-diffusion coefficient can be compared with those of $D_s = 3.1$ meV Å$^{3/2}$ (or $D_s = 4.0$ meV Å^2 for the simple diffusion case) given for the plastic-crystal phase [8], something which serves to evidence the fact that spin fluctuations at least as strong as in the orientationally disordered γ-phase are present in this lower temperature crystal.

As a means of comparison with recent theoretical developments, the wavevector dependence of the linewidths can also be reasonably accounted for by using formulae given for two-dimensional quantum Heisenberg antiferromagnets [19]:

$$\Gamma_Q = \frac{\Gamma_0(1+\alpha Q^2)^{1/2}}{[1+\frac{1}{2}\theta \ln(1+Q^2)]^{3/2}} \tag{8}$$

an expression employed by Tyč and co-workers [19] for the analysis of simulation results for the classical lattice rotor model. The corresponding values for the Γ_0-, α- and θ-parameters are 1.15, 3.66 and −1.13 respectively. A comparison of this set of values with those reported from the simulation [19] indicates that the value of Γ_0 which governs the relaxation rate at $Q = 0$ is not too different from that of 0.85 reported from the simulation or 0.96 resulting from a coupled-mode calculation by Grempel [19]. In contrast, positive but small values are found for $\theta \approx 0.08$, whereas those for α seem to be comparable. In summary, the magnetic spectral responses can also be described by means of recent treatments based on renormalization group analysis for which only the spin-stiffness constant and the perpendicular susceptibility at $T = 0$ K are required as input. The $S_m(Q, \omega)$ response, as commented above, can also be described in hydrodynamic terms and the wavevector dependence of the damping terms follows the same law as that arising from these treatments.

4.3. Thermodynamics

As a means to characterize the nature of the magnetic excitations present in this phase, we have computed the values of the integral

$$\mu \int_0^{E_c} \mathrm{d}E \; Z_m(E) \frac{1}{\exp(E/k_B T) - 1} \tag{9}$$

where μ is taken as the effective number of Bohr magnetons (set to $1.8\mu_B$ as derived from diffraction data [2]), using a cutoff value of $E_c = 20\,\mathrm{meV}$, for the whole range of existence of the β-phase where, due to the short temperature range where it exists, it is expected that $Z_m(E)$ will not show any strong dependence with temperature†. The calculated quantities are proportional to the total magnetic susceptibility measured in macroscopic experiments. The best fit to the values so computed, for a temperature range $24 \leqslant T \leqslant 44\,\mathrm{K}$, closely follows a T^2 law with a coefficient of $1.23 \times 10^{-4}\,\mathrm{K}^{-2}$, somewhat analogous to that observed for the total susceptibility by DeFotis [1]. A behaviour linear in T^2 for the macroscopic parallel susceptibility (or for the difference between perpendicular and parallel components) of an antiferromagnet was found by Kubo [27] several decades ago. The present result can be thus interpreted on the basis of a temperature-independent perpendicular component, so that the ratio of $\chi_\parallel(T)/\chi_\perp$ approximately increases in T^2 as was also evidenced by calculations and experimental measurements in other, somewhat related, antiferromagnetic layered materials [28].

Even if the contribution of magnetic origin to the neutron cross section is relatively large, its relevance in accounting for the thermodynamics of the crystal is rather modest, as can be judged from the argument that follows. The structure-related excitations are accounted for by the $Z(E)$ vibrational density of states calculated from the LD results, and estimates of the relevant thermodynamic functions can therefore be computed by suitable integrations over this function. The value calculated for the structural contribution to the heat capacity‡ for this temperature is $34.41\,\mathrm{J\,K^{-1}\,mol^{-1}}$, which nearly coincides with the calorimetric measurement [29], which gives $34.42\,\mathrm{J\,K^{-1}\,mol^{-1}}$. Such a coincidence seems to be a direct consequence of how the model potential was initially parametrized. On the other hand, a similar calculation employing $Z_m(E)$ gives a magnetic contribution to the specific heat of $4.09\,\mathrm{J\,K^{-1}\,mol^{-1}}$, a value that can be compared with some estimates made by DeFotis [1] in the vicinity of the α–β transition. The estimate for the magnetic entropy as calculated using this frequency distribution is of about $0.3R$, which is far below that of $1.099R$ ($R \ln 3$) corresponding to an orbitally non-degenerate triplet ground state [1]. The dependence of both quantities with temperature, for the whole range of existence of the β-phase, is finally plotted in figure 8. The interesting thing to note is that, although the magnetic contribution to the entropy (figure 8(*b*)) seems to follow a linear temperature dependence, the best function found to approximate the specific heat data was a simplified spin-wave expression

$$C_{mag}(T) = AT^{-1/2} \exp(-E_0/k_B T) \tag{10}$$

where the values found for the physically significant parameter was $E_0 = 4.6(1)\,\mathrm{meV}$. If such quantity is interpreted as the energy gap for the $Q = 0$ magnons, one finds that such a value comes very close (within 0.2 meV) to that calculated by Meier [30] for a distorted triangular lattice as commented above.

† Only in the near vicinity of the magnetoelastic β–α transition (i.e. below 26 K) are strong deviations from smooth behaviour expected to occur due to the increasing importance of magnetoelastic couplings. See for instance [26]

‡ Calculated from the $Z(E)$ arising from the LD calculations and normalized to $6R$, as shown in figure 7.

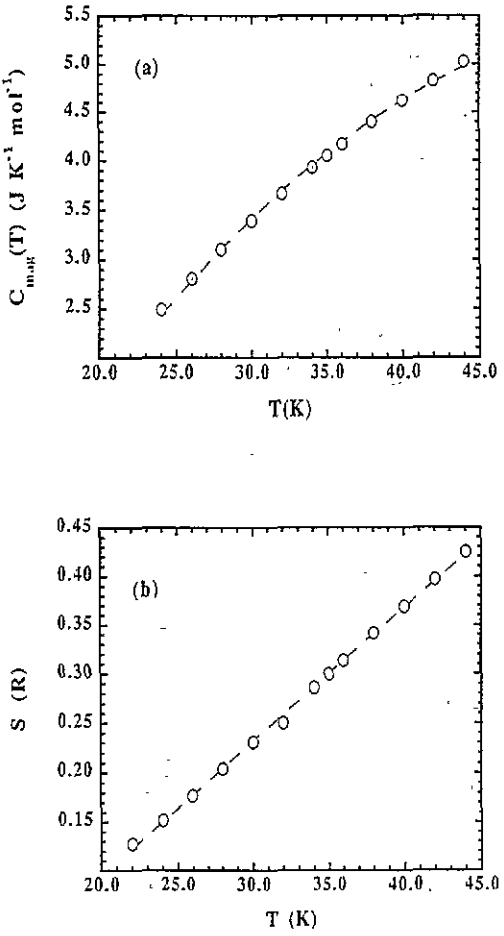

Figure 8. (*a*) Temperature dependence of the magnetic contribution to the heat capacity, as estimated from the $Z_m(E)$ function. Open circles are calculated data, and the broken curve gives the approximation in terms of the simplified spin-wave model (see text). (*b*) Temperature dependence of the magnetic entropy. Units are given in terms of the gas constant and the broken curve corresponds to the best approximation using a linear law.

4.4. Final remarks

As a main general conclusion, the present work has provided evidence that the peculiar magnetic behaviour of β-oxygen can be traced back to microscopic scales, since quantities directly derived from microscopic probes are able to account for the antiferromagnetic-like behaviour observed in macroscopic experiments. The presence of static magnetic short-range order is then established, and therefore the physics of this interesting magnetic material should be describable in terms of phenomena occurring at length-scales not larger than those corresponding to two unit cells.

Finally, the present results can serve to understand the origin of the depolarization curves measured by μSR at zero field [4]. The shape of those curves are reminiscent of those found for noble metals doped with paramagnetic rare earths (Gd or Er) [31,32]. The presence of strong spin diffusion in both the β- and γ-phases can thus account for the shape of the depolarization curves and due account of these facts as well as longitudinal muon spin relaxation data will be given soon.

Acknowledgments

This work has been supported in part by DGICYT grant no. PB89-0037-C03. Helpful

discussions with Dr F Dunstetter from the Laboratoire de Solides Irradies are gratefully acknowledged. The help of the staff of the Institut Laue–Langevin during the performance of the experimental measurements is gratefully acknowledged.

References

[1] de Fotis G C 1981 *Phys. Rev.* B **23** 4714
[2] Collins M F 1966 *Proc. Phys. Soc.* **89** 415
Alikhanov R A 1967 *JETP Lett.* **5** 349
Meier R J and Helmholdt R B 1984 *Phys. Rev.* B **29** 1387
Stephens P W, Birgenau R J, Majkrzak C F and Shirane G 1983 *Phys. Rev.* B **28** 452
[3] Meier R J, Schinkel C J and de Visser A 1982 *J. Phys. C: Solid State Phys.* **15** 1015
[4] Storchak V G, Kirilov B F, Pirogov A V, Duginov V N, Grebinnik V G, Lazarev A B, Ols'shevsky V G, Pomyakushin Yu V, Shilov S N and Zhukov V A 1992 *Phys. Lett.* **166A** 429
[5] Stephens P W and Majkrzak C F 1986 *Phys. Rev.* B **33** 1
[6] Dunstetter F, Plakhti V P and Schweizer J 1988 *J. Magn. Magn. Mater.* **72** 258
[7] Lotkev V M 1979 *Sov. J. Low Temp. Phys.* **5** 142
Slyusarev A, Freiman Y A and Yankelevich R P 1981 *Sov. J. Low Temp. Phys.* **7** 265
Jensen A J P 1986 *Phys. Rev.* B **33** 6352
Meier R J 1985 *Phys. Lett.* **107A** 275
Rastelli E and Tassi A 1986 *J. Phys. C: Solid State Phys.* **19** L423
[8] Chahid A, Bermejo F J, Enciso E, Garcia-Hernandez M and Martinez J L 1993 *J. Phys.: Condens. Matter* **5** 423; 1992 *Europhys. Lett.* **20** 71
[9] Criado A, Conde A and Marquez R 1984 *Acta Crystallogr.* A **40** 696
[10] Alonso J *et al* 1991 *Institut Laue–Langevin Technical Report No* 91AL01T
[11] Johnson M W 1974 *AERE Report No* 5697
[12] Rieutord F *Institut Laue–Langevin software*
[13] Bermejo F J, Alonso J, Criado A, Mompean F J, Martinez J L, Garcia-Hernandez M and Chahid A 1992 *Phys. Rev.* B **46** 6173
[14] Wette F W and Rahman A 1968 *Phys. Rev.* **176** 784
[15] Dunstetter F 1988 *PhD Thesis* Université de Paris-Sud
[16] Rastelli E and Tassi A 1989 *Physica* B **156–157** 115; 1988 *J. Phys. C: Solid State Phys.* **21** 1003
[17] Lovesey S W 1986 *Theory of Neutron Scattering from Condensed Matter* vol 2 (Oxford: Oxford Science Publications) p 317
[18] Cuccoli A, Tognetti V and Lovesey S W 1990 *J. Phys.: Condens. Matter* **2** 3339
[19] Hayden S M, Aeppli G, Mook H A, Cheong S W and Fisk Z 1990 *Phys. Rev.* B **42** 10220
Tyč S, Halperin B and Chakravarty S 1989 *Phys. Rev. Lett.* **62** 835
Grempel D R 1988 *Phys. Rev. Lett.* **61** 1041
[20] Domer B 1992 *Physica* B **180** 265
Fåk B and Domer B 1992 *Institute Laue–Langevin Technical Report No* 92FA008S
[21] Korenbilt I Ya and Shender E F 1988 *Spin Waves and Magnetic Excitations (Modern Problems in Condensed Matter Sciences 22)* vol 2, ed A S Borovik-Romanov and S K Sinha (Amsterdam: North-Holland) p 124
[22] Buchenau U 1985 *Z. Phys.* B **58** 181
[23] Kirkpatrick S and Harris A B 1975 *Phys. Rev.* B **12** 4980
Tahir-Kheli R A 1972 *Phys. Rev.* B **6** 2826
[24] Wormer P E S and van der Avoird A 1984 *J. Chem. Phys.* **81** 1929
Meier R J 1984 *PhD Thesis* Amsterdam University, p 57
[25] Lantwin C J 1990 *Z. Phys.* B **79** 47
[26] Kuchta B, Luty T and Meier R J 1987 *J. Phys. C: Solid State Phys.* **20** 585
[27] Kubo R 1952 *Phys. Rev.* **87** 568
[28] Patashinskii A and Pokrovskii V L 1979 *Fluctuation Theory of Phase Transitions* (Oxford: Pergamon) p 153
[29] Fagerstroem D H and Hallis-Hallet A C 1969 *J. Low Temp. Phys.* **1** 3
[30] Meier R J 1985 *Phys. Lett.* **112A** 341
[31] Schenck A 1985 *Muon Spin Rotation Spectroscopy, Principles and Applications in Solid State Physics* (Bristol: Adam Hilger) ch 5
[32] Brown J A, Heffner R H, Hutson R C, Kohn S, Leon M, Olsen C E, Schillaci M E, Dodds S A, Estle T L, Vanderwater D A, Richards M and McMasters O O 1991 *Phys. Rev. Lett.* **47** 261